minerals

MDPI

Article

Jurassic Uranium-Thorium Deposit of Peralkaline Granitic Rocks, Bokan Mountain, Prince of Wales Island, Southeastern Alaska

Jaroslav Dostal

Department of Geology, Saint Mary's University, Halifax, NS B3H 3C3, Canada; jarda.dostal@smu.ca

Abstract: The Lower Jurassic (ca. 177 Ma) Bokan Mountain granitic complex, located on southern Prince of Wales Island, southernmost Alaska hosts a high-grade uranium-thorium deposit with past production. The complex is a circular body (~3 km in diameter) which intruded Paleozoic granitoids as well as metasedimentary and metavolcanic rocks of the Alexander Terrane of the North American Cordillera. This shallow seated intrusion, which is composed of fractionated peralkaline granites, is a zoned body with a dominant core of arfvedsonite granite and a rim of aegirine granite. All the rock-forming minerals typically record a two-stage growth history and aegirine and arfvedsonite were the last major phases to crystallize from the magma. Both arfvedsonite and aegirine granites have overlapping compositions. The rocks have high contents of rare earth elements, Th, U and high field strength elements (Zr, Nb, Hf and Ta) and low contents of Sr, Ba, Eu and Ti, typical of peralkaline granites. The complex hosts structurally controlled rare metal mineralization, which is associated with the late-stage of magma evolution and hydrothermal fluids. Fluorine complexing played a role during the transportation of rare metals in hydrothermal fluids. The U-Th deposit, which occurs at the margin of the aegirine granite zone, includes structurally controlled shear zone-hosted lenses and irregularly shaped pipe-like orebodies. U-Th mineralization is associated with desilicified and albitized granitic rocks and includes mainly uranothorite and uraninite. These minerals mostly form small ovoids in veinlets typically 0.1 to 1 mm wide. The mine produced about 77,000 t of ore at a grade of ~0.76% U_3O_8 and 3% of ThO_2. The parent magma of the pluton was likely derived from a metasomatized lithospheric source (mantle or lower crust), which was enriched by subduction related processes during Paleozoic time.

Keywords: peralkaline granite; Alaska; uranium; thorium; rare earth elements; deposit; Bokan Mountain

check for updates

Citation: Dostal, J. Jurassic Uranium-Thorium Deposit of Peralkaline Granitic Rocks, Bokan Mountain, Prince of Wales Island, Southeastern Alaska. *Minerals* **2023**, *13*, 1032. https://doi.org/10.3390/min13081032

Academic Editor: Massimo D'Antonio

Received: 29 May 2023
Revised: 26 July 2023
Accepted: 28 July 2023
Published: 31 July 2023

Copyright: © 2023 by the author. Licensee MDPI, Basel, Switzerland. This article is an open access article distributed under the terms and conditions of the Creative Commons Attribution (CC BY) license (https://creativecommons.org/licenses/by/4.0/).

1. Introduction

Peralkaline granitic rocks are relatively rare rock-types, which are commonly enriched in rare elements (rare earth elements (REE), radioactive elements (uranium and thorium]) and high field strength elements (HFSE) such as Nb, Ta, and Zr). This enrichment can be of economic significance and has been a focus of recent exploration [1–3]. However, the origin of such mineralization is controversial. It has been ascribed to extensive fractional crystallization (e.g., [4–6]), late-stage magmatic-hydrothermal processes or low-temperature external hydrothermal fluids [7–9] or a combination of the processes [10–13]. To contribute to these discussions, this paper investigates the Bokan Mountain complex (BMC), a small peralkaline granitic intrusion in a southeastern part of Alaska, which hosts a high-grade uranium-thorium deposit with past production, as well as clusters of felsic dikes, which contain significant REE mineralization. The dikes occur along the margins or adjacent to the BMC in shear zones. The REE mineralization is distinct and ~1.5 km away from the uranium deposit, although both mineralization types are genetically related to the Bokan intrusion. Like other REE deposits associated with peralkaline felsic rocks, the Bokan REE

mineralization is enriched in heavy REE as well as Y relative to total REE, while the Bokan uranium deposit is rich in Th.

Bokan Mountain (lat. 54°55′ N, long. 132°09′ W) is in southeastern Alaska, close to the southern end of Prince of Wales Island (the southernmost major island of Alaska). The complex is an approximately circular Jurassic intrusion (~177 Ma old) about 3 km in diameter, composed of highly fractionated peralkaline granitic rocks. The post-tectonic intrusion is well exposed and displays many geological characteristics typical of extension-related peralkaline granitic complexes worldwide (e.g., [14–17]). The purpose of this paper is to review the available information on the BMC and its U-Th mineralization and to present new whole-rock geochemical data in order to constrain the origin and significance of the U-Th mineralization. A model for Bokan Mountain will be useful to evaluate the petrogenesis and mineralization of similar but less studied alkali felsic igneous bodies in southeastern Alaska and elsewhere. The focus of this paper is on the U-Th deposit. The nature of the REE mineralization of the BMC was discussed in some detail by Dostal et al. [18,19] and Dostal and Shellnutt [20].

2. Geologic Setting and Petrography

BMC lies within the Alexander Terrane of the North American Cordillera (Figure 1). The Cordillera consists of allochthonous oceanic and pericratonic terranes that were accreted to the northwestern margin of Laurentia (the North American craton) between late Paleozoic and early Cenozoic time (e.g., [21]). The Alexander terrane is a large outboard allochthonous terrane, which is considered to have an exotic nature with respect to the Laurentian margin (e.g., lack paleontological affinities with North America; [22,23]). The terrane (Figure 1) was accreted to the North American craton by the middle Cretaceous (~115–95 Ma), well after the emplacement of the Bokan complex.

The basement of southern Prince of Wales Island is composed of the Neoproterozoic to Lower Cambrian Wales Group made up of arc-related volcanic rocks, sedimentary rocks and granitoid intrusions, which were all metamorphosed during the Middle Cambrian to Early Ordovician Wales orogeny. These rocks were unconformably overlain by Ordovician–Early Silurian oceanic arc-related metavolcanic and metasedimentary rocks and intruded by plutons composed mainly of Late Ordovician to Early Silurian quartz monzonites, quartz diorites, diorites and gabbros. The Paleozoic units were metamorphosed during the Klakas orogeny (Middle Silurian to earliest Devonian; [26]). These rocks, which represent an oceanic arc complex [26], host the Bokan stock. Mesozoic rocks are rare in this part of the terrane. Early Jurassic igneous rocks in the Alexander terrane are limited to the BMC, the Dora Bay pluton composed of peralkaline granites and syenite and located about 30 km N of the BMC and bimodal Moffat volcanic rocks 100 km to SE of the BMC (Figure 1), all dated at ~175–185 Ma [25,27].

The Bokan Mountain pluton is a typical anorogenic granitic complex, emplaced at a shallow depth. It produced the contact metamorphic assemblages which included andalusite (chiastolite)-bearing hornfels. Around the intrusion, the Paleozoic country rocks, particularly granitoids, are albitized. A wide (>1 km; [28]) aureole of albitization was produced by infiltration of hydrothermal fluids related to the pluton.

The Bokan granites have variable grain size, ranging from fine to coarse-grained. They are composed typically of quartz and feldspars with 2–10 vol.% of mafic minerals (sodic amphibole-arfvedsonite and sodic clinopyroxene-aegirine in various proportions). Locally, the mafic minerals comprise about 30 vol.% of the rocks. The granites are mainly made up of quartz (~25–45 vol.%), K-feldspar (20–30 vol.%) and albite (30–50 vol.%). The intrusion (Figure 2) is composed of two main zones [29,30]: (1) a core made up of arfvedsonite-bearing granite (porphyry) that forms the main part of the body and (2) an outer ring comprised predominantly of aegirine-bearing granite. The aegirine granite forms a nearly complete circular zone around the core [29,31]. A transition unit between these two zones is composed of aegirine-arfvedsonite granite and is typically about 15 m wide. In addition, there is a discontinuous outermost border zone composed of pegmatitic pods with aegirine

and arfvedsonite crystals enclosed in aplitic rocks. Fine-grained aegirine granite, which outcrops in the central part of the stock probably represents the preserved roof of the intrusion [5]. The intrusion is associated with the quartz-feldspatic (felsic) dikes, which occur throughout the intrusions as well as outside, mainly along shear or fault zones. The dikes, composed mainly of quartz, albite and K-feldspar, form elongated lenses, which are steeply dipping and commonly 0.1 to 3 m thick. They include both aplitic and pegmatitic types. Most of them are rich in REE, Nb, Ta, Zr, Pb, Th and U and are closely related to the Bokan intrusion [18,19,32].

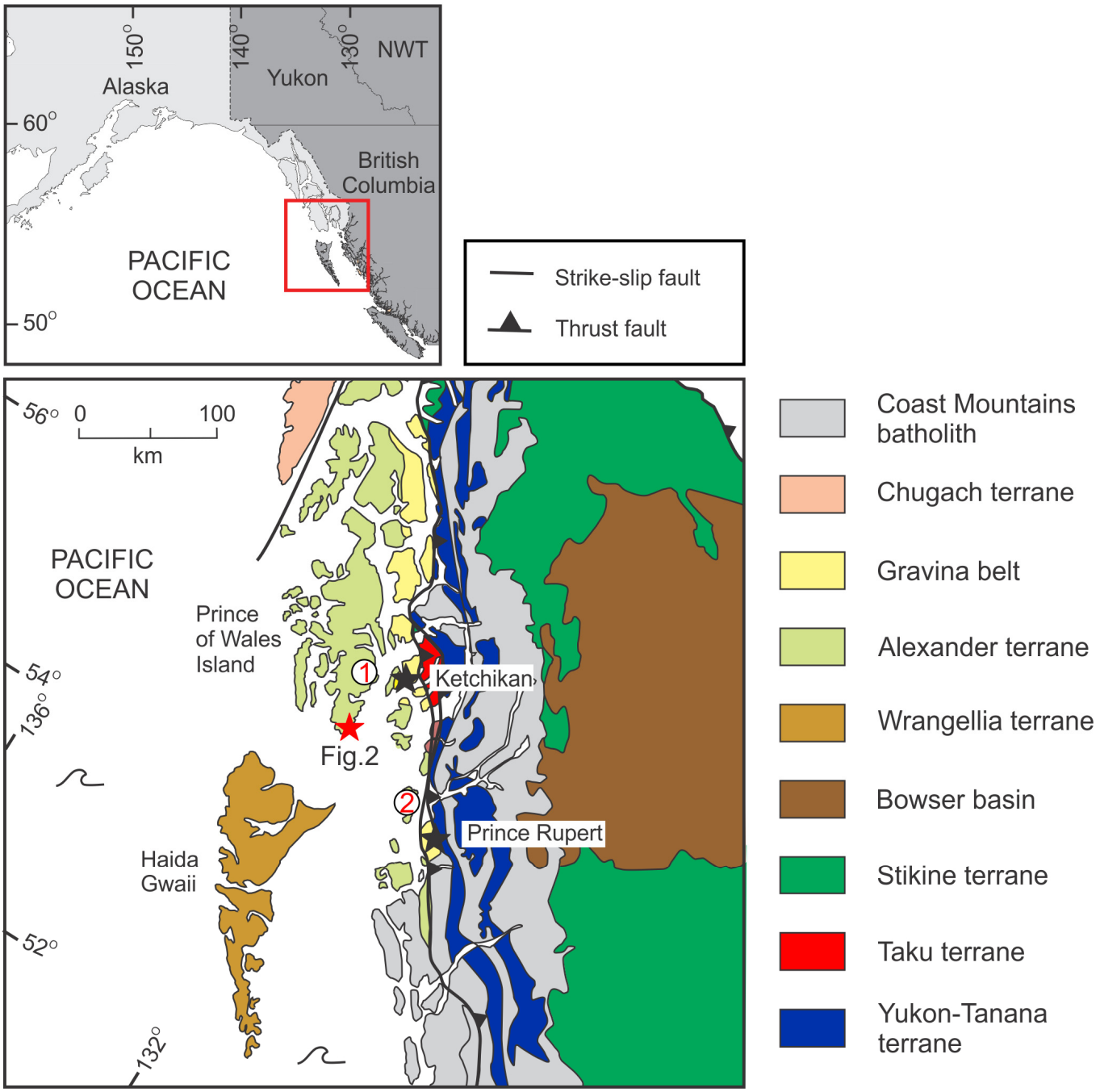


Figure 1. Terrane map of southeastern Alaska and west coast of British Columbia (modified after [24,25]). The map shows the location of Figure 2, the geological map of the Bokan Mountain Complex, southern Prince of Wales Island. The insert shows the location of Figure 1. Sites: 1—Dora Bay pluton; 2—Moffat volcanic rocks.

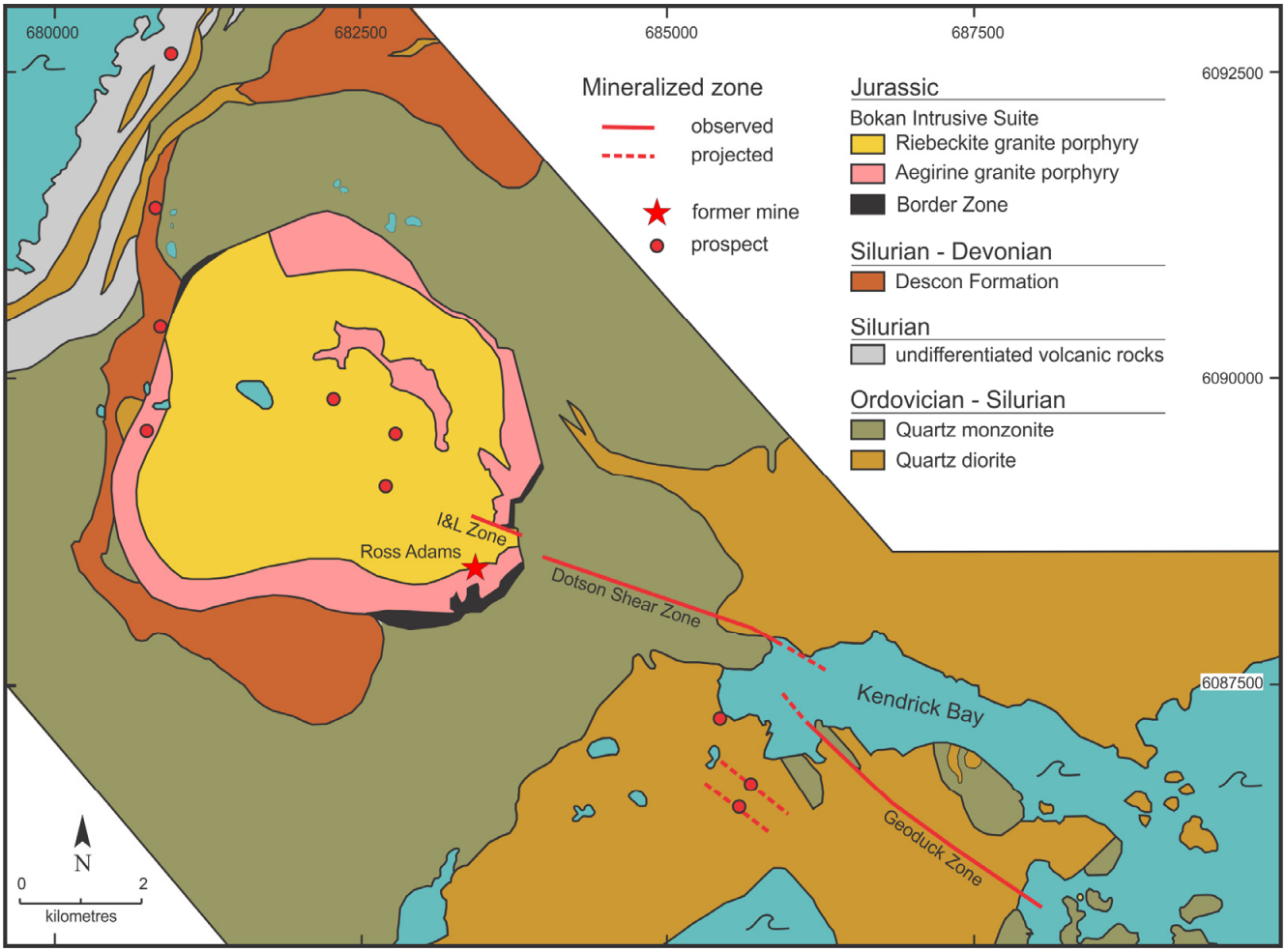


Figure 2. Geological sketch map of the Bokan Mountain complex and surrounding area showing the location of the former Ross-Adams mine and mineralization prospects including mineralized zones. Most promising are Dotson Shear and I&L zones (modified after [19,25,29–31]).

The granitic rocks have diverse texture although two main textures are dominant—primary porphyritic and late protoclastic [5,18,29]. The porphyritic texture contains phenocrysts of subhedral to euhedral quartz that ranges from 5 to 20 mm in diameter and K-feldspar enclosed in a fine-to medium-grained groundmass made up of quartz, albitic feldspar and minor K-feldspar. The protoclastic textures are characterized by broken phenocrysts of quartz and feldspars, bending of feldspar twining and pronounced undulose extinction of quartz crystals. Protoclastic textures resulted from an overpressure of fluids generated during the exsolution of the vapor phase from the magma during late stages of crystallization [5].

K-feldspar occurs as microperthite and cross-hatched microcline while plagioclase (An < 10) forms both a separate phase or an intergrowth or replacement of K-feldspar. Albite pervasively replaces K-feldspar, both in phenocrysts and in the groundmass [18,19]. The groundmass is dominated by albite and quartz with subordinate K-feldspar where the primary assemblage is overprinted by the metasomatic assemblage. All the major minerals have formed during at least two stages, one magmatic and the other related to late-stages (late magmatic to post-magmatic). Albite ranges from magmatic crystals to late- to post-magmatic albitic growth from a fluid phase. The albite is generally euhedral without signs of alteration. Quartz has also crystallized during two stages, initially, as the early megacrysts and then in the matrix and as veinlets. Well-developed early quartz crystals were intruded by the quartz veinlets of the second generation. There are also at least two

generations of K-feldspar. Early K-feldspar, now occurring as a cross-hatched microcline, is enclosed/embayed by microperthitic K-feldspar that is the main K-feldspar phase. Around the Ross-Adam deposit, Cuney and Kyser [5] recognized two stages of alteration of the granites. The first stage included albitization of K-feldspar followed by the second stage, where albitization was accompanied by quartz dissolution leading to the generation of secondary syenitic rocks. This rock type is composed primarily of albite and aegirine with accessory fluorite, monazite, zircon and Fe-Ti oxides. The U-Th mineralization is closely associated with the syenitic rock [5,33,34]. The ore zone appears to be a strongly altered syenitic rock.

The sodic amphibole (arfvedsonite) occurs as subhedral prismatic crystals 1–4 mm long, which are distinctly pleochroic (lilac to blue) and interstitial. It also displays at least two-stages of growth. The inclusion-rich amphibole cores (stage 1) are surrounded an inclusion-free overgrowths (stage 2). Amphibole is commonly replaced by a mixture of secondary minerals (frequently hematite and quartz) or by fibrous aegirine and hematite with interstitial quartz and minor fluorite. Aegirine forms a variety of crystal shapes ranging from equant to prismatic or skeletal. Like arfvedsonite, it also shows a two-stage growth history. Philpotts et al. [32] argued that some aegirine grains might be of hydrothermal origin. Pyroxene and amphibole may be spatially associated but in other samples only one or the other is present. Where both minerals are present, the anhedral to euhedral amphibole partly encloses and corrodes the pyroxene but in some cases pyroxene post-dates amphibole. This association suggests overlapping crystallization of these two minerals. Amphibole and pyroxene are poikilitic, enclosing crystals of quartz, microcline and albite. Individual major rock forming minerals display only limited chemical variations [18,32]. Granitic rocks of the BMC host numerous accessory mineral phases. Particularly common are zircon, monazite, xenotime, titanite, fluorite and Fe-Ti oxides. Some of the accessory minerals including monazite could be late/post-magmatic.

The analyzed rocks from a wider vicinity of the Ross-Adams mine were subdivided into four groups—unaltered granites (group 1), albitized granites (group 2), mineralized albitized granites (group 3) and syenites (group 4) although there are transitions among the groups. Group 2 differs from group 1 by distinct albitization. Albite pervasively replaces K-feldspar, both phenocrysts (especially along the fractures and cleavage planes) and grains in the groundmass. The groundmass is dominated by albite and quartz. The accessory mineralogy appears to be the same as in group 1. Group 3 contains notably higher amounts of accessory minerals. In addition to ubiquitous accessory minerals such as zircon, monazite, xenotime, titanite, fluorite and Fe-Ti oxides, more than twenty U-Th-, REE- and HFSE-bearing minerals have been identified at the Bokan complex (e.g., [19,32,35]). Some of these minerals are variably present in mineralized altered granites and may occur in two or more generations. Group 4 includes a syenite, a fine-grained rock, which is likely the result of albitization and desilicification of the rocks in the proximity of the mineralization [5]. Quartz occurs in this rock only in subordinate amounts.

3. History of Mining and Exploration

After the 1955 uranium discovery in shear zones of the BMC by airborne and subsequently ground surveys [29], mining commenced in 1957 mainly due to incentive programs provided by the US Atomic Energy Commission [36,37]. The uranium mine was in operation intermittently between 1957 and 1971 and produced roughly 77,000 metric tons of ore averaging about 0.76 wt.% U_3O_8 and 3 wt.% ThO_2 [35,37,38]. These concentrations are among the highest grades of U and Th ores ever mined in the United States and the Bokan is the only uranium deposit to have been mined in Alaska. The uranium ore was mined initially in a small open pit (50 × 110 × 7 m deep [36,37] located on the southeastern flank of Bokan Mountain at the Ross-Adams site (Figure 3). As the irregular cylindrical-shaped ore body plunges steeply at the end of pit, the deposit was subsequently developed as an underground operation through the establishment of two haulage adits (mine entrances). Ore was shipped by barge from the property to continental U.S. for

processing, to fulfill contracts with the U.S. Atomic Energy Commission [1]. The mine stopped operations in 1971, due to depressed prices for uranium, leaving some uranium ore in the ground [38]. Subsequently, several companies carried out exploration in the BMC area during 1971–1981 [33,37,38].

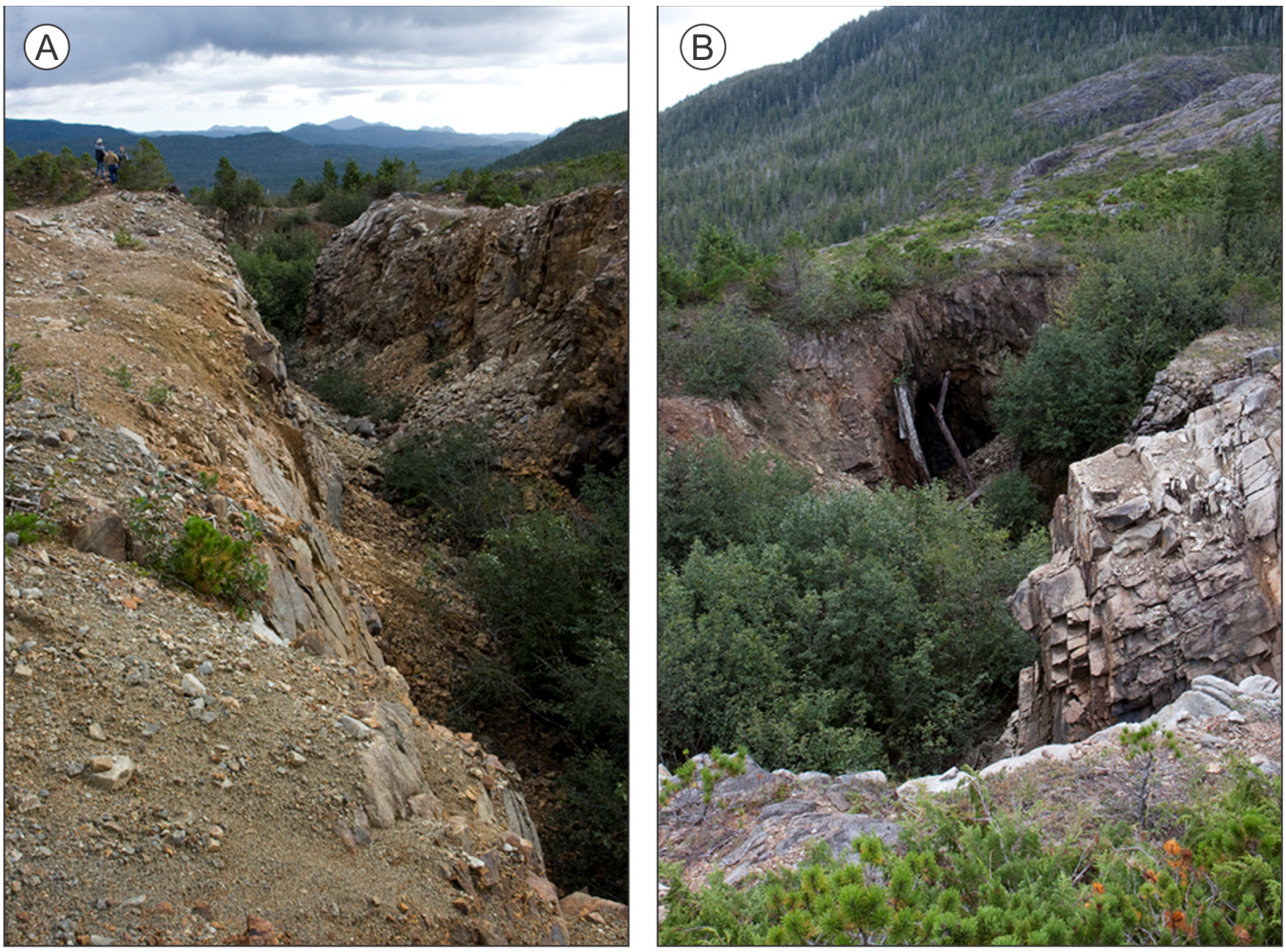


Figure 3. (**A**) Abandoned Ross-Adams open-pit mine; (**B**) A southern part of the Ross-Adams pit mine with an adit. Host granites show distinct fracture-cleavages parallel to faults, which controlled emplacement of the deposit.

In addition to the Ross-Adam site, historic exploration has resulted in the delineation of several mineral prospects within or proximal to the BMC, some of which contained significant levels of REE, Y, Zr and Nb, in addition to U and Th [29,35,38]. Warner and Barker [38] predicted important resources of Th, REE, Y, Zr, Nb and Ta in the complex, in addition to potentially commercial resources of uranium remaining in and around the Ross-Adams mine.

After several years of hiatus, new exploration activities started in 2007 and continued to the present. The exploration targets shifted from uranium to REE and particularly focused on a prospect called the Dotson zone, a cluster of felsic dikes more than 2 km long (Figure 2), which lies just outside (within 1 km) of the Bokan stock [19]. The mineral resource estimation for the REE ore at the Dotson zone yielded 4.9 million metric tons of ore containing 0.61 wt.% oxides of REE and Y with a high ratio of heavy REE/total REE (heavy REE + Y/total REE + Y = ~0.6; [39]).

4. Mineral Prospects/Deposits

The BMC hosts structurally controlled rare metal mineralization, which is associated with the late stage of magma evolution and hydrothermal fluids. Warner and Barker [38] recognized two types of economically important prospects: (1) the Ross-Adams deposit and (2) mineralized dike systems associated with shear/fault zones (Figure 2), in particular the I&L and Dotson prospects [18,19,25,28,38]. Most mineralized zones appear to define a NW-trending corridor that cuts the Bokan complex.

The first type, the Ross-Adams deposit (the site of a former uranium mine), which occurs at the southeastern margin of the aegirine granite zone, includes structurally controlled shear zone-hosted lenses and irregularly shaped pipe-like orebodies. The main ore pipe is up to 24 m in diameter and is offset by several faults. The ore body has an irregular cylindrical shape and was mined along strike for over 300 m. The pipe contained a high-grade ore surrounded by a lower grade (<0.5 wt.% U_3O_8) ore zone, 0.6–6 m wide, which was not mined [37]. U-Th ore also occurs as lenses/pods in en echelon NW-striking shear zones in aegirine granite near the Ross-Adams mine. The lenses are up to 30 m long and 3 m wide [33,34]. At present, the size of the remaining deposit is not known. There is no reliable information available on the continuation of the ore body below the lower audit (Figure 4).

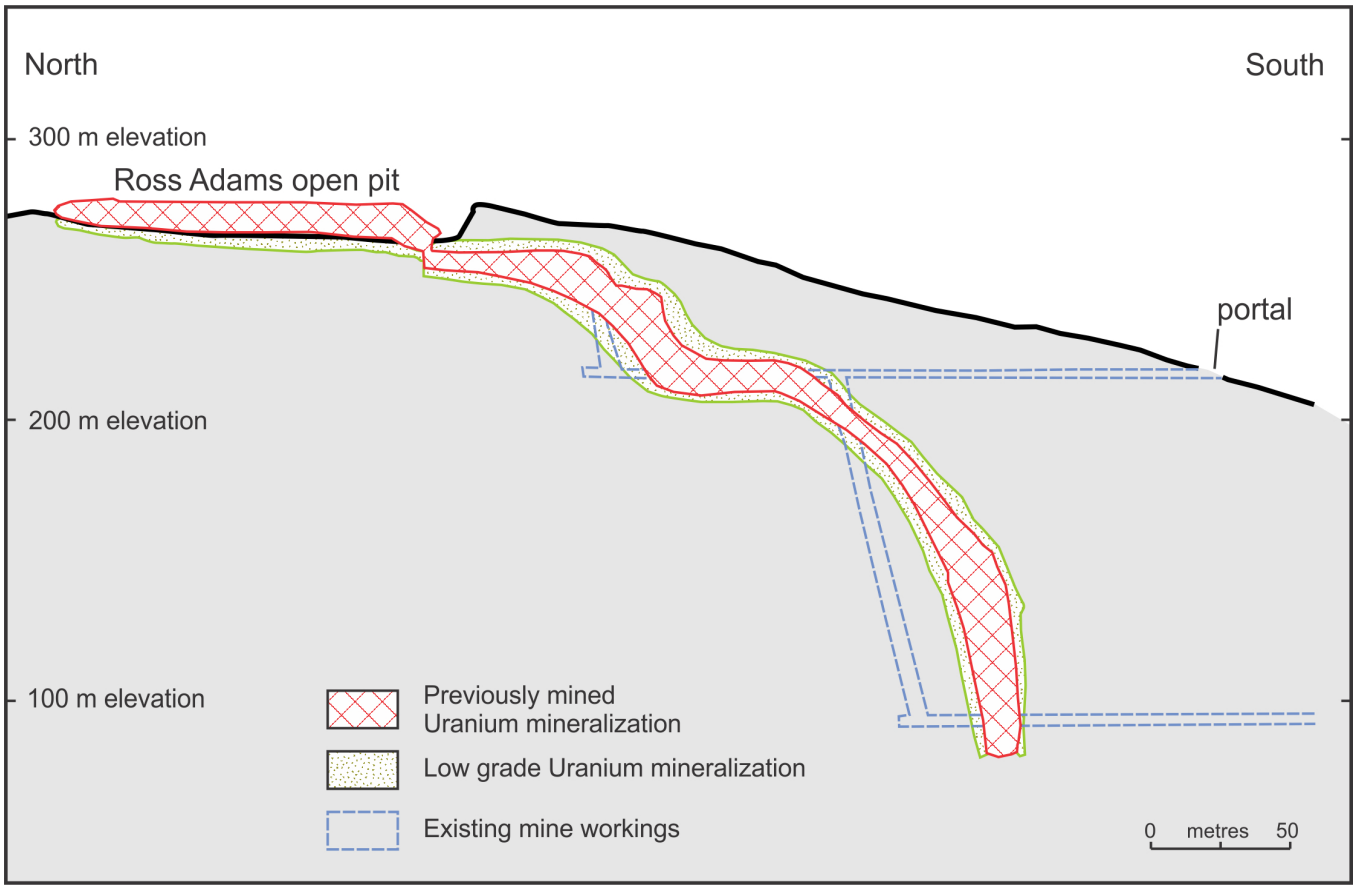


Figure 4. Cross-section of the main ore pipe of the Ross-Adams deposit showing the previously mined ore (>0.5 wt.% U_3O_8), lower grade ore (<0.5 wt.% U_3O_8) and mine workings. Modified after Keyser and McKenney [37].

The ore pipe is associated with aegirine syenite, composed mainly of albite and aegirine but appears to be structurally controlled. The ore bodies contain microfractures generated by rapid late-stage magmatic degassing. The microfractures are ore-bearing veinlets containing U-Th minerals [29]. The ore resembles strongly altered host granite/syenite

with numerous ore-bearing veinlets typically between 0.1 and 1 mm thick. The main ore minerals are uranothorite and uraninite [33,34]. The dominant uranothorite forms small ovoids 0.2 to 2 mm in size with crystals, which are typically 30 to 500 μm long [5]. Hematite forms fine veinlets or rims around the ovoids. Gangue minerals are aegirine, albite, quartz, hematite, calcite, fluorite, chlorite, clay minerals and sulfides [29]. Sulfides (pyrrhotite, pyrite, galena, sphalerite, chalcopyrite, molybdenite) are disseminated but rare (<2%). Secondary uranium minerals are sparce and include gummite, sklodowskite, beta-uranophane, bassetite and novacekite [33,35]. The mineralization at the Ross-Adams deposit is accompanied by wall-rock alteration that includes intense albitization, chloritization and the calcite-fluorite or quartz-hematite replacement of aegirine. Hematitization occurs in the outer parts of the ore zones and locally marks the position of shear zones [33,34].

The second type of mineralization occurs in felsic dikes (vein-dikes of Warner and Barker [38] and Philpotts et al. [32]). The earliest mineralization was late magmatic but shows significant hydrothermal overprints and contains the bulk of known REE-Y and Nb resources of the Bokan complex [18,19]. Unlike the Ross-Adams deposit, which lies within the intrusion, this mineralization occurs both inside (but along the margins) and outside the Bokan stock (in adjacent country rocks). Various structural features of the BMC and related dikes as well as the geochronology indicate the contemporaneity of the emplacement of the BMC, the alteration and rare metal mineralization at the Ross-Adam deposit and the Dotson and I&L zones [25,29,33,40].

5. Geochronology

The granitoid rocks which occur in close proximity of the BMC are of Middle Ordovician to Early Silurian age. Lanphere et al. [41] reported K-Ar ages of 431 ± 21 and 446 ± 22 Ma for hornblende from nearby granitic rocks from southeast of the BMC. Armstrong [42,43] obtained a Rb-Sr whole-rock age of 432 ± 19 Ma for the granitic country rocks while U-Pb zircon dating of Gehrels and Saleeby [26] and Gehrels [30] of several granitoid rocks outcropping in the vicinity of the BMC yielded ages ranging from 480 to 438 Ma. Dostal et al. [25] also reported a U-Pb zircon age of 469.2 ± 3.0 Ma from a quartz monzonite outcropping near the Dotson Zone. All these data are consistent with an age range obtained from the graptolites and conodonts of country metasedimentary rocks [44].

The Bokan stock is of Jurassic age. No clear and sharp magmatic contacts between the two main zones of the pluton have been observed; these units pass transitionally into each other over a distance of about 15 m, although the aegirine granite is assumed be slightly older [31,33]. Taylor et al. [40] reported U-Pb zircon ages for the outer aegirine rim of 182 ± 2.7 and 179.9 ± 2.0 Ma, respectively, while for the arfvedsonite core they obtained Ar-Ar amphibole ages of 181.9 ± 1.8 and 177.7 ± 1.5 Ma. Dostal et al. [25] published a U-Pb zircon age of 177.2 ± 0.2 Ma and an Ar-Ar amphibole age of 175.5 ± 0.6 Ma for the arfvedsonite granite. These ages are consistent with Cuney and Kyser [5] who argued that petrographic variations (aegirine and arfvedsonite granitic zones) resulted from differences in crystallization conditions. This suggestion is also supported by the close geochemical similarities between these units [5,19].

Thompson et al. [45] obtained a K-Ar albite age of 182 Ma for granite/syenite of the Ross-Adams deposit. Dostal et al. [25] also reported an Ar-Ar amphibole plateau age of 176.3 ± 0.8 Ma from a granitic dike associated with uranium mineralization. DeSaint-Andre and Lancelot [46] obtained a U-Pb zircon age of 101 ± 3 Ma for the U-Th mineralization and 167 + 7/−5 Ma for the emplacement of the complex. However, the ages of the mineralization of the BMC are uncertain as the primary mineral assemblages were overprinted by younger late magmatic and post-magmatic hydrothermal events. Furthermore, the mineralization is hosted in shear zones whose reactivation commonly results in resetting of the radiogenic ages (many accessory minerals including zircon and monazite occur in multiple generations in the BMC). It is not clear if various younger ages of mineralization (e.g., [40,46]) represent separate later events including a reactivation of shear zones.

6. Analytical Methods

Whole-rock major and trace elements (Supplementary Table S1) were determined using lithium metaborate–tetraborate fusion at the Activation Laboratories Ltd. In Ancaster, Ontario, Canada. Major elements were analyzed by an inductively coupled plasma-optical emission spectrometer whereas trace elements were determined by an inductively coupled plasma-mass spectrometer. Replicate analyses of the reference standard rocks indicate that the 1 sigma errors are between 2% and 8% of the values cited. The detection limits and information on the major and trace element analyses are available at the Activation Laboratories web site (www.actlabs.com). The four groups of BMC rocks (unaltered granites—group 1; albitized granites—group 2; mineralized albitized granites—group 3; syenites—group 4) have also distinct geochemical characteristics. Groups 2 and 3 have $Na_2O/K_2O > 3$, group 3 has either Th > 300 ppm or U > 40 ppm and group 4 has <68 wt.% SiO_2. Some of the analyses in Supplementary Table S1 were previously published in Dostal and Shellnutt [20].

Nd isotopic ratios of three granite samples (Table 1) were determined at the Atlantic Universities Regional Facility at the Department of Earth Sciences of Memorial University of Newfoundland (St. John's, Newfoundland, Canada) using procedures described by Pollock et al. [47]. Replicate analyses of Jndi-1 yield a mean $^{143}Nd/^{144}Nd = 0.512100 \pm 6$. Neodymium depleted mantle model ages (T_{DM}; Table 1) were determined according to DePaolo [48].

Table 1. Nd isotopic composition of Bokan granitic rocks.

Sample		Age (Ma)	Nd (ppm)	Sm (ppm)	$^{147}Sm/^{144}Nd$	$^{143}Nd/^{144}Nd_{(m)}$	2σ	$^{143}Nd/^{144}Nd_{(i)}$	$\varepsilon_{Nd}(t)$	T_{DM} (Ma)
757	granite	177	44.4	9.30	0.1267	0.512834	7	0.512687	5.4	395
758	granite	177	92.1	22.7	0.1491	0.512851	5	0.512678	5.2	485
777	granite	177	120	29.2	0.1472	0.512842	8	0.512672	5.1	491

$^{143}Nd/^{144}Nd(m)$ are measured values; $^{143}Nd/^{144}Nd(i)$ and $\varepsilon_{Nd}(t)$ are age-corrected to 177 Ma; T_{DM}-depleted mantle age calculated according to DePaolo [48].

7. Geochemistry of the Pluton

The granitic rocks of the Bokan Mountain pluton are silica rich (Figure 5), have high contents of $Fe_2O_{3(t)}$ (~3.5–6 wt.%) and alkalis (~7–10 wt.%) but are low in CaO (<0.6 wt.%) and MgO (<0.06 wt.%) and have a high Fe/Mg ratio (Figure 5). According to the R1-R2 multicationic diagram [49], the rocks are alkali granites (Figure 5). They are peralkaline with an agpaitic index [molar $Al_2O_3/(Na_2O + K_2O)$] < 1 (0.81–0.88). Their main variations of major elements are associated with changes in relative modal proportions of albite and K-feldspar and with the contents of mafic minerals. The rocks have high contents of fluorine [5,32] as also reflected by widespread occurrence of fluorite. Like many peralkaline granites, they are high in REE, Y, HFSE, Pb, Th and U but are low in Ba (<80 ppm) and Sr (<40 ppm). The chondrite-normalized REE patterns of the Bokan peralkaline granites are typically slightly enriched in LREE with $(La/Sm)_N$ ~ 2–3 but have variable HREE as also reflected in the $(La/Yb)_N$ range of 1–4. However, on average, these rocks show slight LREE enrichment and a relatively flat HREE segment (Figure 6). The chondrite-normalized REE patterns of all these rocks feature a distinct negative Eu anomaly with Eu/Eu* ~ 0.3. Primitive mantle-normalized trace element plots (Figure 6) display enrichment in Th, U, Pb, Rb, Zr and Hf but distinct depletion in Sr, Ba, P, Eu and Ti. Both REE and mantle-normalized plots of the Bokan granites are comparable to many other typical A-type peralkaline granites (e.g., [3,12,17]). There is no obvious geochemical difference between arfvedsonite granites and aegirine granites suggesting that the mineralogical contrasts are mainly related to differences in crystallization conditions [5,19].

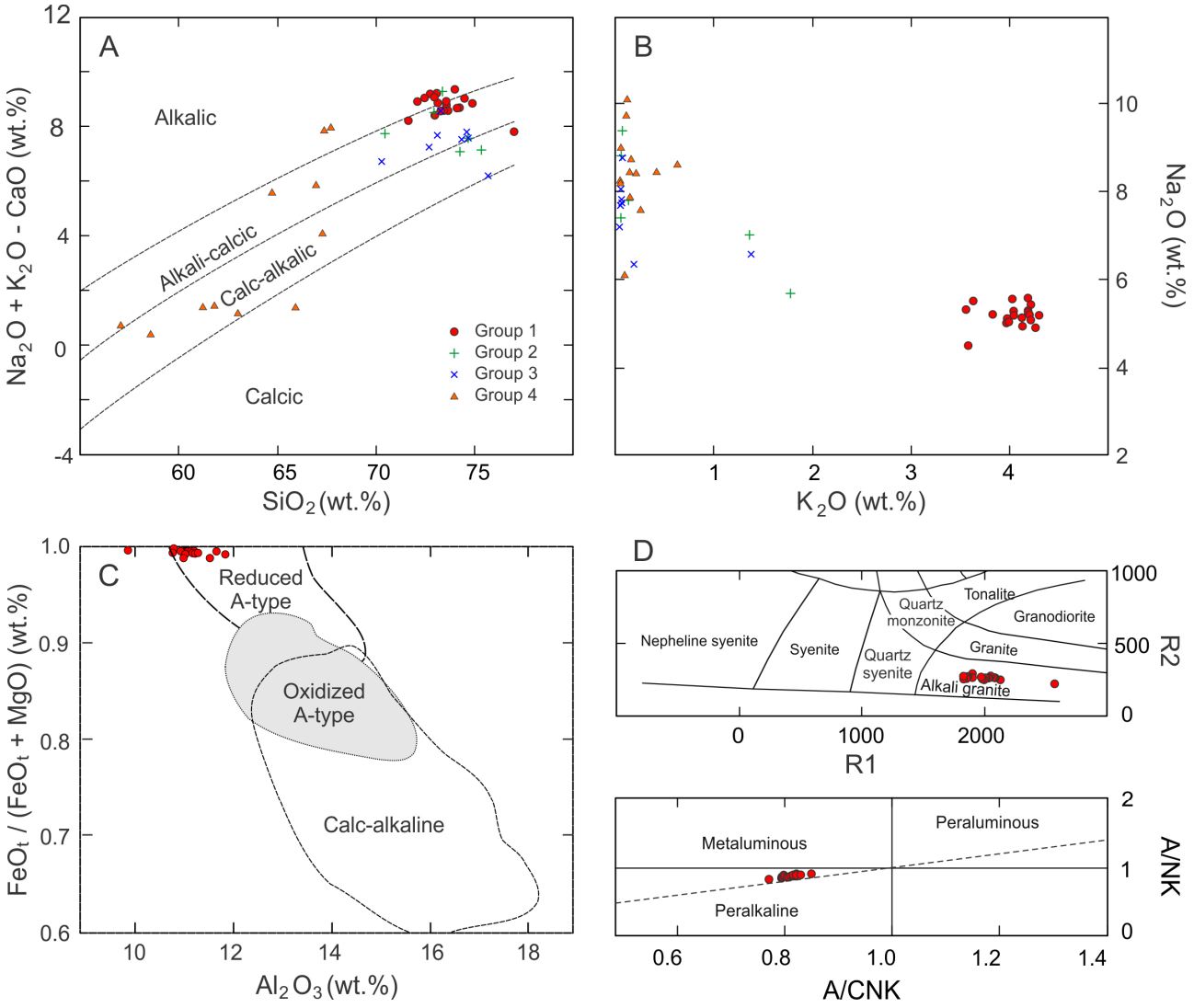


Figure 5. Major element characteristics of the BMC rocks from the vicinity of the Ross-Adams mine area. (**A**) MALI (modified alkali-lime index) diagram: Plot of (Na_2O + K_2O-CaO) versus SiO_2 (wt.%) showing the ranges of alkalic, alkali-calcic, calc-alkalic and calcic rock series after Frost et al. [50]; (**B**) Na_2O versus K_2O (wt.%) diagram; (**C**) $FeO_t/(FeO_t + MgO)$ versus Al_2O_3 (wt.%) diagram showing compositional fields of reduced and oxidized A-type granites and calc-alkaline granites after Dall'Agnol and de Oliveira [51]; (**D**) upper: Multielement classification plot of De La Roche et al. [49] [R1: 4Si − 11(Na + K) − 2(Fe + Ti); R2: 6Ca + 2Mg + Al]; lower: Plot of molar $Al_2O_3/(Na_2O + K_2O)$ [A/NK] versus $Al_2O_3/(CaO + Na_2O + K_2O)$ [A/CNK] that discriminates metaluminous, peraluminous and peralkaline compositions of granitic rocks.

Nd isotopic ratios for the peralkaline granites from the vicinity of the Ross-Adams site are given in Table 1 where they are age-corrected to the age of emplacement at 177 Ma. The data are comparable to those of Dostal et al. [18,19] and Philpotts et al. [32] from the pluton and the Dotson and I&L dikes. The high positive ε_{Nd} values (mostly +5 to +6) are consistent with derivation of all these rocks from the same source, probably depleted but metasomatized upper mantle. Thus, the intrusion and dikes are closely genetically related. Nd isotopic data imply that the magma and source were not contaminated by old continental crust. The lithospheric source was metasomatically enriched probably in the early Paleozoic, as suggested by neodymium depleted mantle model ages ([48]; Table 1). The model ages of the peralkaline granites are roughly like the emplacement ages of the older regional arc-related granitoids [19,25,26,30,32]. The initial enrichment of the source in

incompatible elements including U and Th by subduction processes may have significantly contributed to high concentrations of these elements in the peralkaline melts.

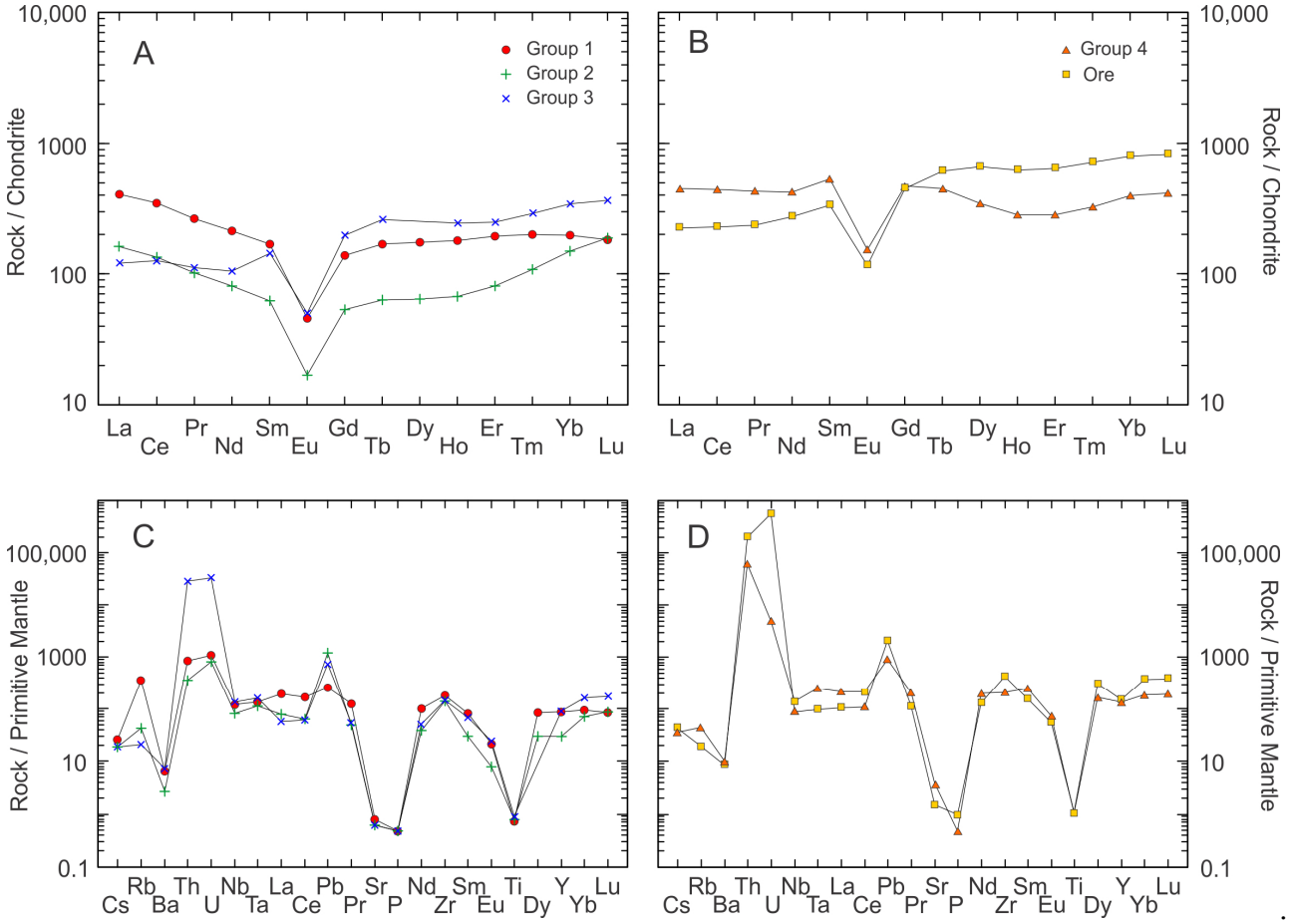


Figure 6. (**A**,**B**) Chondrite-normalized REE plots of averages of the four rock groups and ore from Ross-Adams mine area. (**A**): groups 1, 2 and 3; (**B**): group 4 and ore. Normalizing values after [52]. (**C**,**D**) Primitive mantle-normalized trace element plots of averages of the four rock groups and ore from Ross-Adams mine area. (**C**): groups 1, 2 and 3; (**D**): group 4 and ore. Normalizing values are after [53]. Elements are arranged in the order of decreasing incompatibility from left to right.

8. Alteration/Metasomatism

The altered rocks, which occur around the Ross-Adams deposit, include the albitized non-mineralized (group 2) and mineralized (group 3) granites and syenites (group 4). Syenitic rocks have variable compositions. They have SiO_2 typically between 57 and 68 wt.%, high Na_2O (6–10 wt.%) but low K_2O (<0.3 wt.%) and MgO (<0.4 wt.%). The rocks of the ore zone resemble syenitic rocks (Table 2).

The element transfers responsible for compositional differences between peralkaline granite and altered rocks (albitized mineralized and non-mineralized granites, syenites and ore) can be appraised using the combined isocon/Pearce element ratio approach proposed by Hilchie et al. [54]. This method improves visualization of element behavior, as portrayed on spider diagrams. The main challenge, as is commonly the case with altered rocks, is identifying relatively unaltered precursors against which modified rocks can be compared. In the Ross-Adams case, the mean composition of peralkaline granite from the vicinity of the U-Th deposit (Group 1, ST1) is compared with albitized mineralized and non-mineralized granites, syenites and ore, assuming Ti is a conserved element. As the granites (groups 1–3) have an overlapping range of TiO_2 contents, it was assumed that their average Ti contents are the same. The result (Figure 7) indicates that compared to peralkaline granites, the altered felsic rocks are depleted in Si, Al and K and enriched in

Na. This is consistent with evidence for sodium metasomatism (albitization) of these rocks. An enrichment of syenites in Ca is probably due to the presence of secondary calcite. The results also indicate that the ore is similar to the syenitic rocks although it does not contain a notable amount of secondary calcite.

Table 2. Average whole-rock compositions of groups from the Ross-Adams mine area.

n	**20**		**7**		**8**		**12**		**3**
(wt.%)	**Group 1**		**Group 2**		**Group 3**		**Group 4**		**Ore**
	aver	stdv	aver	stdv	aver	stdv	aver	stdv	
SiO_2	73.56	1.11	73.62	1.64	73.56	1.66	63.61	3.61	64.03
TiO_2	0.15	0.02	0.15	0.09	0.18	0.05	0.21	0.09	0.22
Al_2O_3	10.98	0.35	10.39	2.32	1.37	0.26	12.93	1.44	12.37
Fe_2O_3	4.46	0.51	6.01	2.67	4.94	0.70	4.33	2.13	7.34
MnO	0.08	0.04	0.12	0.08	0.12	0.07	0.14	0.09	0.29
MgO	0.03	0.01	0.01	0.01	0.03	0.02	0.15	0.11	0.17
CaO	0.38	0.09	0.32	0.12	0.29	0.10	6.13	4.15	0.39
Na_2O	5.19	0.25	7.53	1.29	7.54	0.80	8.42	1.02	7.74
K_2O	4.03	0.22	0.63	0.73	0.24	0.46	0.17	0.16	0.07
P_2O_5	0.01	0.00	0.01		0.01		0.01	0	0.02
LOI	0.44	0.27	0.39	0.24	0.70	0.41	1.47	0.32	2.32
Total	99.9		99.19		98.97		97.56		94.96
(ppm)									
Be	6.35	1.5	9.14	4.3	9.63	1.69	12.75	2.9	
Zn	300	108	517.1	415	270	119	268.3	199	
Ga	38.8	1.5	42.71	8.2	40.25	2.5	48.25	5.3	
Rb	217	29.7	29.0	34.2	12.5	27.0	26.67	22.9	11.63
Sr	15.7	9.1	12.86	10.5	12.38	9.21	76.92	31.6	29.67
Y	372.1	469	141.7	155.4	388.0	385	580.9	221	649.7
Zr	1898	1200	1534	943	1550	1278	2161	2005	4520
Nb	79.65	38.4	57.71	29.6	87.75	42.2	91.83	90.2	58.33
Sn	22.1	10.2	19.43	16.3	26.38	7.98	12.42	13.2	
Cs	0.54	0.23	0.40	0.20	0.40	0.20	0.75	0.60	0.90
Ba	44.40	33.7	19.43	16.3	48.25	36.5	66.58	130	56.10
La	126.3	49.2	56.84	58.5	37.46	29.0	138.2	160	69.37
Ce	280.9	115.3	122.1	125.6	101.9	83.6	357.2	336	182.7
Pr	32.44	13.2	14.07	15.0	13.69	12.4	52.26	44.4	28.7
Nd	127.8	54.1	54.27	58.2	63.34	63.9	250.6	208	163
Sm	32.92	15.1	13.51	14.8	28.18	32.3	103.1	92.4	64.5
Eu	3.38	1.71	1.38	1.57	3.69	4.16	11.15	9.59	8.47
Gd	35.95	21.1	15.34	18.5	50.93	60.4	120.6	96.2	115
Tb	8.04	5.99	3.3	3.99	12.41	14.1	21.26	14.9	28.9
Dy	56.31	49.7	22.47	26.0	84..68	91.6	111.2	69.7	210
Ho	12.92	12.9	5.26	5.52	17.56	17.7	20.19	10.9	44.00
Er	40.52	41.7	18.04	15.9	52.33	45.5	58.78	28.3	133.3
Tm	6.48	5.91	3.65	2.54	9.43	6.3	10.5	5.83	22.8
Yb	41.22	30.5	31.67	20.3	71.71	38.4	81.96	51.1	165.7
Lu	5.87	3.60	6.02	4.02	11.82	5.96	13.22	8.75	26.3
Hf	44.72	27.6	37.27	23.1	36.28	29.4	55.99	51.1	19.4
Ta	5.04	2.00	4.53	2.14	6.08	3.03	9.28	10.1	3.57
Pb	39.33	41.8	198.1	464	109.5	133	137.8	203	313
Th	67.60	61.2	29.79	20.0	2330	2838	4827	5324	15,900
U	21.90	9.94	17.51	7.95	673.7	663.4	97.87	68.0	11,153

Note: n = number of samples; aver = average; stdv = standard deviation.

The chondrite-normalized REE plots of the albitized granites are variable ranging from those with $(La/Yb)_N > 1$ to those with the ratios < 1 although they still have a similar negative Eu anomaly ($Eu/Eu^* \sim 0.3$). On average, the albitized non-mineralized granites show a negative slope for LREE [$(La/Sm)_N > 1$] but a positive slope for HREE [$(Gd/Yb)_N < 1$]. On the other hand, albitized mineralized granites have on average a flat LREE segment

with $[(La/Sm)_N \sim 1]$ but are enriched in HREE. Both syenites and ore have significantly higher REE contents than the granites. The chondrite normalized plot of the average ore shows a positive slope with $(La/Yb)_N$, $(La/Sm)_N$ and $(Gd/Yb)_N < 1$ (Figure 6).

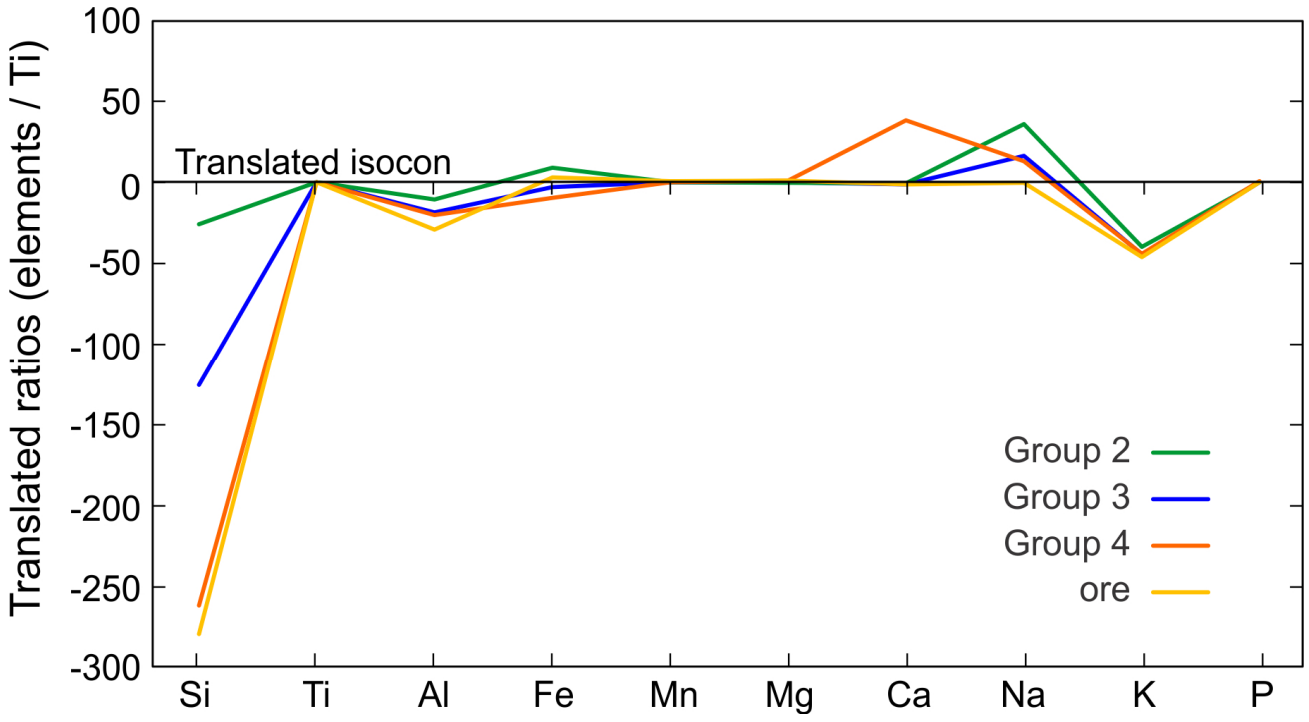


Figure 7. Unified isocon/PER diagram of Hilchie et al. [54] comparing the average composition of Ross-Adams altered felsic rocks (albitized granite, mineralized albitized granite, syenite and ore) with peralkaline granite, assuming the immobility of Ti during alteration and metasomatism. Elements plotting above the translated isocon line were added; those below it were removed. The addition of Na and removal of Si, Al and K characterized metasomatism of the Ross-Adams rocks.

The mantle-normalized plots for mineralized albitized granites display more distinct positive anomalies for Th, U and Pb but negative ones for Ba, Sr, K, Ti and Eu. Otherwise they are similar to those of the other albitized granites. In fact, the shapes of the patterns of all altered rocks are similar although the positive anomalies of Th, U and Pb are significantly larger in mineralized rocks particularly ore and syenite (Figure 6).

9. Zircon Saturation Thermometry

Saturation temperatures of some accessory minerals, in particular zircon and monazite, in the peralkaline granites of BMC can provide magma temperature estimates, which are useful to constrain petrogenetic and thermal histories. These data can be used to constrain the temperature in magmatic liquids whose composition fall within the experimental calibration range. Gervasoni et al. [55] modified the procedure of Watson and Harrison [56] and Boehnke et al [57] for the calculation of zircon saturation temperatures (T_{Zr}) so that it can be also used for peralkaline granites. The average of calculated temperatures of Gervasoni et al. [55] for group 1 granites (eliminating samples with Zr > 2000 ppm) is high, around 943 °C, reflecting high solubility of Zr in alkaline magmas, which significantly increases with increasing alkalinity of the melts, particularly in F-rich systems.

Miller et al. [58] argued that "hot" granites ($T_{Zr} > 800$ °C) are anhydrous high temperature rocks whereas "cold" granites ($T_{Zr} < 800$ °C) were derived from a crustal source in water-fluxed environments. The results suggest that the initial magmatic temperature at which zircon crystallized was characteristic of anhydrous magmas [58].

10. Discussion

10.1. Emplacement

The Bokan granite was considered to represent a top part of a larger magmatic complex emplaced at a shallow depth [5]. Thompson [33] inferred that the initial intrusion was of oxidized granitic magma of the marginal zone (aegirine granite) and was followed by the development of a separate volatile phase rich in U, Th, REE and HFSE in the magma chamber. Subsequent collapse of the roof of the magma chamber triggered rapid degassing of the magma chamber and the escape of fluids and highly fractionated melts. Magma at that time was fluid saturated [5,33]. Expulsion of fluids and melts from the deeper central part of the pluton was focused into the zones of structural weakness, mainly around the southeastern margin of the pluton and led to the formation of the U-Th deposit, a generation of the dike systems and deposition of rare metal-bearing minerals in the dikes. This event was followed by the intrusion of the dominant core of the pluton in rapid series, perhaps overlapping intrusive events. The emplacement sequence is consistent with relative ages of the units [33,40].

Magma devolatization was accompanied by a decrease in oxygen fugacity [5]. Lower pressure and less oxidizing conditions led to a transition from aegirine to arfvedsonite granite [33]. The lack of distinct geochemical differences and the absence of sharp magmatic contacts between these two zones support a short time interval between the intrusive events. Microfracturing of the rocks around the Ross-Adams deposit was probably produced during this late magmatic devolatization of the magma chamber. Enclaves of host metamorphic rocks and aegirine granites in the central upper part of the pluton probably represent roof pendants of the collapsed magma chamber [5]. MacKevett [29] argued that the initial mineralization was coeval with the intrusions of dikes.

10.2. Petrogenesis

The Bokan granitic rocks are peralkaline A-type granites (Figure 8) with alkali amphibole and alkali pyroxene in the mode. The granites are highly differentiated (Figure 8) with high contents of HREE, HFSE, Pb, Th and U as well as halogens (F), but low contents of Sr, Ba, Ti and P. The rocks of the pluton show only limited variations in the major element composition. They also have overlapping high positive Nd isotopic values suggesting a close genetic link among all these rocks and derivation from the same magma. Dostal and Shellnutt [20] inferred that the Bokan granitic rocks were generated from alkali or transitional basaltic magmas by extensive fractional crystallization. In turn, the parent magma was probably formed by partial melting from a lithospheric source (mantle or lower crust) metasomatically enriched in rare metals. Although the granites are peralkaline, they plot into the A2-group granite field (Figure 8B) on the classification diagrams of Eby [59], probably reflecting the metasomatic HREE and Y enrichment of their source as suggested by the significant variations in the abundances of these elements.

Protracted fractional crystallization was influenced by high concentrations of alkalis and fluorine in the magma that led to an increase in the solubility of rare metals in volatile-bearing peralkaline felsic melts and to the curbing of crystallization of rare metal-bearing accessory minerals until late stages of fractionation [9,11,60,61]. Low solid–liquid partition coefficients of typical rock-forming minerals for these elements in the peralkaline melts also add to their enrichment during fractional crystallization (e.g., [62,63]). The depletion of Ba, Sr and Eu on the primitive mantle-normalized plots attests to the fractionation of feldspars. Feldspar fractionation is also supported by the variations in Rb/Sr versus Sr in the granitic rocks of group 1 (Figure 8). The negative Ti anomaly is likely due to the fractionation of Fe-Ti oxides and titanite whereas the negative P anomaly is likely a result of apatite fractionation.

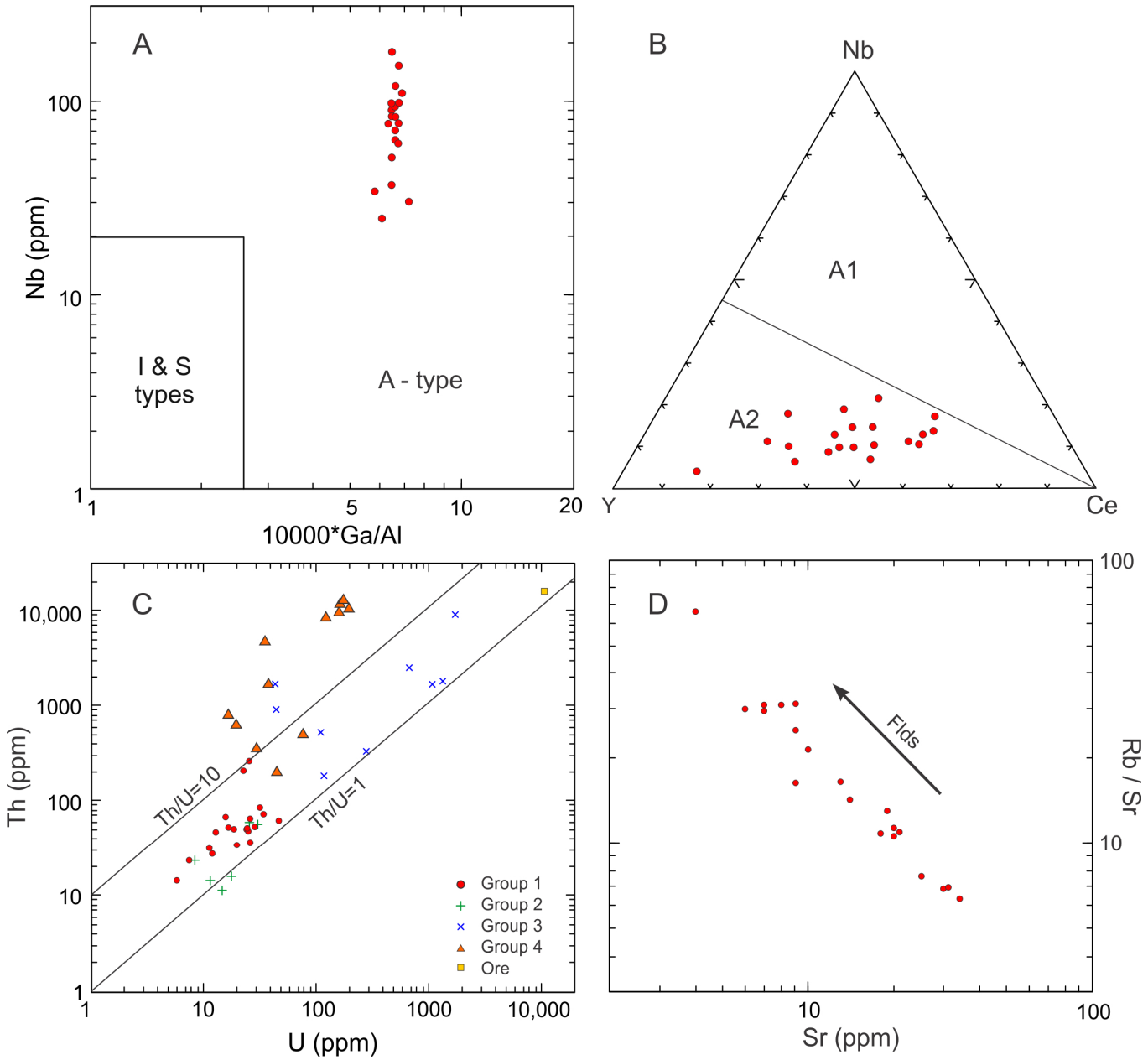


Figure 8. (**A**) 10,000 × Ga/Al versus Nb (ppm) diagram (after Whalen et al. [60]) for the BMC granitic rocks of group 1, classifying them as A-type rocks. Fields: I&S field is for I- and S-type granites while the A field is for the A-type granites. (**B**) Y-Nb-Ce ternary diagram of Eby [59] for BMC peralkaline granites of group 1. (**C**) Variations in Th versus U (ppm) for the BMC rocks from the vicinity of Ross-Adams mine site. (**D**) Rb/Sr versus Sr (ppm) for granites of group 1. Vector depicts the fractionation trend of the compositional changes in the residual liquid when the primary alkali feldspar is progressively removed from the magma during the fractional crystallization. Felds-feldspars.

Granitic rocks of both aegerine and arfvedsonite zones of the stock and of the dikes have chondrite-normalized REE patterns showing distinct negative Eu anomalies. The Eu anomalies, which result from the separation of feldspars, indicate extensive fractional crystallization. The Bokan felsic rocks are unusual as they all show very similar depletion (Eu/Eu* = ~ 0.3). The similarity of the Eu anomalies in granites and dikes [19] suggests that they were formed at the same stage of the magma evolution and at that stage, europium anomalies had stopped evolving in these rocks because conditions became sufficiently

oxidizing for the europium to be in the trivalent state when entering into feldspars. Figure 9 shows that the variations in Ba and La/Yb do not correlate with Eu/Eu* indicating that further crystallization took place under oxidizing conditions.

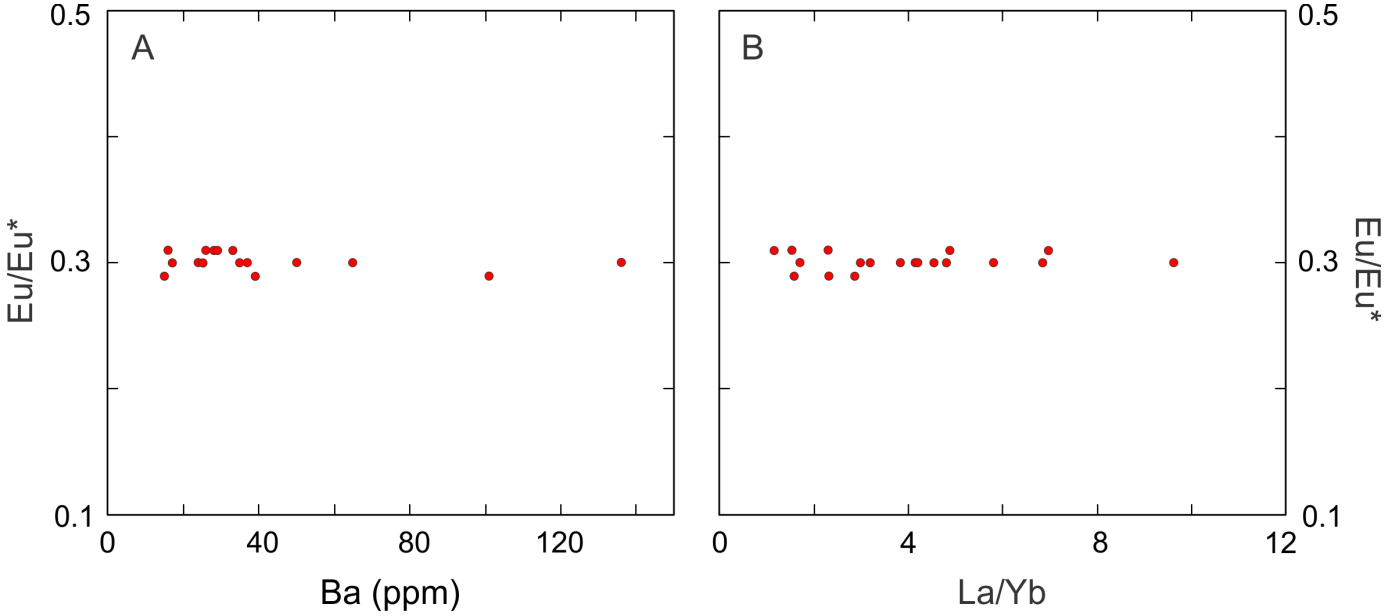


Figure 9. Variations of (**A**) Ba (ppm) and (**B**) La/Yb versus (Eu/Eu*) in the BMC granitic rocks of Group 1. Eu/Eu* = $Eu_N/[(Sm_N{*}Gd_N)]^{0.5}$.

The modest variations in major elements in the granites contrast with significant variations in trace elements, suggesting that these two groups of elements were decoupled during the evolution of the Bokan granitic complex (Table 2). The lack of obvious correlations among various rare metals and the differences in the trace element patterns among the rocks with comparable major elements suggest an important role for fluids and accessory minerals during the fractionation processes particularly during the late stages. As in many other peralkaline granites (e.g., [10,64,65]), the bulk of rare metals in the Bokan granitic rocks are hosted in ore/accessory minerals and their distributions reflect the interaction of melts/rocks with coexisting fluids. The presence of fluorite in the granitic rocks indicates that the fluids were F-rich and facilitate complexing and mobility of rare metals. Rare metals such as U and Th can be transported as fluoride complexes [65].

10.3. Origin of Mineralization

The origin of the rare metal mineralization related to peralkaline granitic rocks is still under discussion (e.g., [3,10,12,16]). The two most frequently invoked models are magmatic and hydrothermal. However, at the BMC, both magmatic and hydrothermal processes played a role during the mineralization, which was a protracted event and involved two or more stages.

Fractional crystallization likely occurred in the deeper part of the magma chamber, during which the magma became highly fractionated and fluid saturated. Subsequently, fluids were released from the hotter and deeper part of the magma chamber and migrated towards the cooler marginal part of the intrusion. Highly fractionated melts and fluids enriched in rare metals escaped and followed zones of weakness. These fluids produced mineralization as well as extensive microfracturing and alteration of the granites. Fluids and melts also penetrated the country rocks along fractures and shear zones up to several km from the intrusion. The exogranitic mineralization in dikes hosted by the country rocks (e.g., Dotson) differs from that hosted by the stock (Ross-Adams). The sites in the country rocks are poorer in U and Th and their REE patterns show slight enrichment in LREE.

The association of mineralization with the altered part of the complex and dikes, the post-magmatic (hydrothermal) characteristics of many ore minerals and replacement textures suggest that the bulk of mineralization is related to hydrothermal activities. Younger hydrothermal processes that remobilized and enriched the rare metals (U, Th, REE, HFSE) produced new mineral assemblages which overprinted the primary magmatic mineral associations. Mineralization is mostly associated with structurally controlled alteration zones where post-magmatic hydrothermal fluids could circulate. Recent geochronological data on the BMC [40] indicate that the hydrothermal processes probably took place over a longer period of time (10–12 m.y.). As the rare metal mineralization at the BMC is located mainly along shear zones, it is not clear whether a protracted period of mineralization represents reactivation or a new mineralization pulse.

11. Conclusions

Peralkaline granites are an important host of rare metal deposits, particularly of heavy REE, Y, Nb, Ta, Th and U. The origin of such deposits, emplaced in extension-environment, requires a multistage process. In the BMC, their formation involved several distinct factors and events. The first event was the melting of a metasomatically enriched mantle/lower crustal source followed up by extensive magmatic differentiation leading to the formation of a highly fractionated magma with a commensurate build-up of volatiles. The next event was late-magmatic mineralization associated with the release of metal-rich fluids. The fluids migrated into structurally prepared zones where the bulk of the mineralization occurs. Subsequently, post-magmatic and hydrothermal fluids remobilized and enriched the rare metal mineralization.

There are other peralkaline felsic intrusions with elevated concentrations of rare metals that have the potential for hosting rare metal mineralization in the southern part of Prince of Wales Island [33,66–69]. They include the Jurassic Dora Bay pluton, located about 30 km north of Bokan Mountain, which yielded an age of 182.2 ± 5.5 million years [70], and is similar in size and composition to the BMC. Collectively, this mineralization may reflect the presence of enriched lithospheric mantle or lower crust under this part of the Alexander terrane [71] and suggests that the area may be a metallogenic province. In addition to rare metal mineralization, BMC could be economically important as a source of geothermal energy. BMC granites due to their high concentrations of U, Th and K (e.g., [72]) are good candidates for use in geothermal energy production.

Supplementary Materials: The following supporting information can be downloaded at: https://www.mdpi.com/article/10.3390/min13081032/s1, Table S1: Whole-rock analyses of rocks from Ross Adams mine area.

Funding: U.S. Geological Survey and Ucore Rare Metals Ltd.

Data Availability Statement: All data are contained within this manuscript and corresponding supplementary file.

Acknowledgments: I would like to thank Sue Karl, Harmen Keyser, Jim Barker and Jim Robinson for many valuable discussions and encouragement and to Randy Corney and Mitchell Kerr for technical assistance.

Conflicts of Interest: J. Dostal is a director of Ucore Rare Metals, a company which owns the mineral rights for a part of the Bokan Mountain complex.

References

1. Long, K.R.; Van Gosen, B.S.; Foley, N.K.; Cordier, D. *The Principal Rare Earth Element Deposits of the United States—A Summary of Domestic Deposits and a Global Perspective*; Scientific Investigations Report 2010-5220; U.S. Geological Survey: Reston, VA, USA, 2010; 96p.
2. Verplanck, P.L.; Van Gosen, B.S.; Seal, R.R.; McCafferty, A.E. *A Deposit Model for Carbonatite and Alkaline Intrusion-Related Rare Earth Element Deposits*; Scientific Investigations Report 2010-5070-J; U.S. Geological Survey: Reston, VA, USA, 2014; 58p.
3. Dostal, J. Rare metal deposits associated with alkaline/peralkaline igneous rocks. *Rev. Econ. Geol.* **2016**, *18*, 33–54.
4. Cuney, M. Felsic magmatism and uranium deposits. *Bull. Soc. Geol. Fr.* **2014**, *185*, 75–92. [CrossRef]

5. Cuney, M.; Kyser, K. Magmatic processes involved in uranium deposit formation. In *Geology and Geochemistry of Uranium and Thorium Deposits*; Cuney, M., Kyser, K., Eds.; Mineralogical Association of Canada, Short Course Series: Quebec City, QC, Canada, 2015; Volume 46, pp. 99–138.
6. Boily, M.; William-Jones, A.E. The role of magmatic and hydrothermal processes in the chemical evolution of the Strange Lake plutonic complex, Quebec/Labrador. *Contrib. Mineral. Petrol.* **1994**, *118*, 33–47. [CrossRef]
7. Salvi, S.; Williams-Jones, A.E. The role of hydrothermal processes in the granite-hosted Zr, Y, REE deposit at Strange Lake, Quebec/Labrador: Evidence from fluid inclusions. *Geochim. Cosmochim. Acta* **1990**, *54*, 2403–2418. [CrossRef]
8. Salvi, S.; Williams-Jones, A.E. The role of hydrothermal processes in concentrating HFSE in the Strange Lake peralkaline complex, northeastern Canada. *Geochim. Cosmochim. Acta* **1996**, *60*, 1917–1932. [CrossRef]
9. Linnen, R.L.; Cuney, M. Granite-related rare-element deposits and experimental constraints on Ta–Nb–W–Sn–Zr–Hf mineralization. In *Rare-element Geochemistry and Mineral Deposits*; Linnen, R.L., Samson, I.M., Eds.; Geological Association of Canada: St. John's, NL, Canada, 2005; Volume 17, pp. 45–68.
10. Salvi, S.; Williams-Jones, A.E. Alkaline granite-syenite deposits. In *Rare-element Geochemistry and Mineral Deposits*; Linnen, R.L., Samson, I.M., Eds.; Geological Association of Canada: St. John's, NL, Canada, 2005; Volume 17, pp. 315–341.
11. Gray, T.R.; Hanley, J.J.; Dostal, J.; Guillong, M. Magmatic enrichment of uranium, thorium and rare earth elements in late Paleozoic rhyolites of southern New Brunswick, Canada: Evidence from silicate melt inclusions. *Econ. Geol.* **2010**, *106*, 127–143. [CrossRef]
12. Dostal, J. Rare Earth Element Deposits of Alkaline Igneous Rocks. *Resources* **2017**, *6*, 34. [CrossRef]
13. Dostal, J.; Gerel, O. Rare Earth Element Deposits in Mongolia. *Minerals* **2023**, *13*, 129. [CrossRef]
14. Bowden, P. The geochemistry and mineralization of alkaline ring complexes in Africa (A review). *J. Afr. Earth Sci.* **1985**, *3*, 17–39. [CrossRef]
15. Bowden, P.; Black, R.; Martin, R.F.; Ike, E.C.; Kinnaird, J.A.; Batchelor, R.A. Niger-Nigerian alkaline ring complexes: A classic example of African Phanerozoic anorogenic mid-plate magmatism. *Geol. Soc. Spec. Publ.* **1987**, *30*, 357–379. [CrossRef]
16. Richardson, D.G.; Birkett, T.C. Peralkaline rock associated rare metals. In *The Geology of North America*; Eckstrand, O.R., Sinclair, W.D., Thorpe, R.I., Eds.; Geological Society of America: Boulder, CO, USA, 1996; Volume P-1, pp. 523–540.
17. Bonin, B. A-type granites and related rocks: Evolution of a concept, problems and prospects. *Lithos* **2007**, *97*, 1–29. [CrossRef]
18. Dostal, J.; Kontak, D.J.; Hanley, J.; Owen, V. *Geological Investigation of Rare Earth Element and Uranium Deposits of the Bokan Mountain Complex, Prince of Wales Island, southeastern Alaska*; U.S. Geological Survey Mineral Resources External Research Program—Report GO9PA00039; U.S. Geological Survey: Reston, VA, USA, 2011; 122p.
19. Dostal, J.; Kontak, D.J.; Karl, S.M. The Early Jurassic Bokan Mountain peralkaline granitic complex (southeastern Alaska): Geochemistry, petrogenesis and rare-metal mineralization. *Lithos* **2014**, *202–203*, 395–412. [CrossRef]
20. Dostal, J.; Shellnutt, J.G. Origin of peralkaline granites of the Jurassic Bokan Mountain complex (southeastern Alaska) hosting rare metal mineralization. *Int. Geol. Rev.* **2016**, *58*, 1–13. [CrossRef]
21. Colpron, M.; Nelson, J.L.; Murphy, D.C. Northern Cordilleran terranes and their interactions through time. *GSA Today* **2007**, *17*, 4–10.
22. Colpron, M.; Nelson, J.L. A Palaeozoic Northwest Passage: Incursion of Caledonian, Baltican and Siberian terranes into eastern Panthalassa, and the early evolution of the North American Cordillera. In *Earth Accretionary Systems in Space and Time*; Cawood, P.A., Kröner, A., Eds.; Geological Society of London: London, UK, 2009; Volume 318, pp. 273–307.
23. Colpron, M.; Nelson, J.L. (Eds.) *Paleozoic Evolution and Metallogeny of Pericratonic Terranes at the Ancient Pacific Margin of North America, Canadian and Alaskan Cordillera*; Geological Association of Canada: St. John's, NL, Canada, 2006; Volume 45, 523p.
24. Nelson, J.L.; Diakow, J.B.; Mahoney, J.B.; van Staal, C.; Pecha, M.; Angen, J.; Gehrels, G.; Lau, T. North Coast project: Tectonics and metallogeny of the Alexander terrane, and Cretaceous sinistral shearing of the western Coast belt. *B.C. Minist. Energy Mines Pap.* **2012**, *1*, 157–180.
25. Dostal, J.; Karl, S.M.; Keppie, J.D.; Kontak, D.J.; Shellnutt, J.G. Bokan Mountain peralkaline granitic complex, Alexander terrane (southeastern Alaska): Evidence for Early Jurassic rifting prior to accretion with North America. *Can. J. Earth Sci.* **2013**, *50*, 678–691. [CrossRef]
26. Gehrels, G.E.; Saleeby, J.B. Geology of southern Prince of Wales Island, southeastern Alaska. *Geol. Soc. Am. Bull.* **1987**, *98*, 123–137. [CrossRef]
27. Karl, S.M.; Barker, J.C.; Dostal, J. Structural controls on emplacement of Early Jurassic peralkaline granite and rare earth mineralization at Bokan Mountain, southeast Alaska. *Geol. Soc. Am. Abstr. Programs* **2014**, *46*, 782.
28. Barker, J.C.; Van Gosen, B.S. Alaska's rare earth deposit and resource potential. *Min. Eng.* **2012**, *64*, 20–32.
29. MacKevett, E.M., Jr. *Geology and Ore Deposits of the Bokan Mountain Uranium-Thorium Area, Southeastern Alaska*; U.S. Goverment Publishing Office: Washington, DC, USA, 1963; Volume 1154, 125p.
30. Gehrels, G.E. *Geologic Map of the Southern Prince of Wales Island, Southeastern Alaska*; Map 1-2169, Scale 1:63,000; U.S. Geological Survey: Reston, VA, USA, 1992.
31. Thompson, T.B.; Pierson, J.R.; Lyttle, T. Petrology and petrogenesis of the Bokan granite complex, southeastern Alaska. *Geol. Soc. Am. Bull.* **1982**, *93*, 898–908. [CrossRef]
32. Philpotts, J.A.; Taylor, C.D.; Tatsumoto, M.; Belkin, H.E. *Petrogenesis of Late-Stage Granites and Y-REE-Zr-Nb-Enriched vein Dikes of the Bokan Mountain Stock, Prince of Wales Island, Southeastern Alaska*; Open File Report 98-459; U.S. Geological Survey: Reston, VA, USA, 1998; 71p.

33. Thompson, T.B. Geology and uranium-thorium mineral deposits of the Bokan Mountain granite complex, southeastern Alaska. *Ore Geol. Rev.* **1988**, *3*, 193–210. [CrossRef]
34. Thompson, T.B. Uranium, Thorium, and Rare Metal Deposits of Alaska. *Econ. Geol. Monogr.* **1997**, *9*, 460–482.
35. Staatz, M.H. I&L uranium and thorium vein system, Bokan Mountain, southern Alaska. *Econ. Geol.* **1978**, *73*, 512–523.
36. Stephens, F.H. The Kendrick Bay project. *West. Min.* **1971**, *44*, 151–158.
37. Keyser, H.J.; McKenney, J. *Geological Report on the Bokan Mountain Property, Prince of Wales Island, Alaska*; NI 43-101 Report; Landmark Minerals Inc.: Toronto, ON, Canada, 2007; 48p.
38. Warner, J.D.; Barker, J.C. *Columbium and Rare Earth-Bearing Deposits at Bokan Mountain, Southeast Alaska*; Open-File Report 33-89; United States Bureau of Mines: Washington, DC, USA, 1989; 196p.
39. Bentzen, E.H.; Ghaffari, H.; Galbraith, L.; Hammen, R.F.; Robinson, R.J.; Hafez, S.A.; Annavarapu, S. *Bokan Mountain Rare Earth Element Project near Ketchikan, Alaska*; Preliminary Economic Assessment—NI 43-101; Tetra Tech.: Vancouver, BC, Canada, 2013; 227p.
40. Taylor, C.D.; Aleinikoff, J.N.; Holm-Denoma, C.S.; Neymark, L.A.; Bala, S.A.; Pascarelli, S.E.; Piller, R.M.; Karl, S.M.; Van Gosen, B.S.; Morgan, L.E.; et al. New geochronologic constraints on the formation and hydrothermal enrichment of the Bokan Mountain peralkaline igneous complex and associated HREE deposits, Southeastern Alaska, USA. *Geol. Soc. Am. Abstr. Programs* **2016**, *48*, 3.
41. Lanphere, M.A.; MacKevett, E.M.; Stern, T.W. Potassium-argon and lead-alpha ages of plutonic rocks, Bokan Mountain area, Alaska. *Science* **1964**, *145*, 705–707. [CrossRef]
42. Armstrong, R.L. Rb-Sr dating of the Bokan Mountain granite complex and its country rocks. *Can. J. Earth Sci.* **1985**, *22*, 1233–1236. [CrossRef]
43. Armstrong, R.L. Rb-Sr dating of the Bokan Mountain granite complex and its country rocks: Reply. *Can. J. Earth Sci.* **1986**, *23*, 744–745. [CrossRef]
44. Eberlain, G.D.; Churkin, M.; Carter, C.; Berg, H.C.; Ovenshine, A.T. *Geology of the Craig Quadrangle, Alaska*; Open-File Report 83-91; U.S. Geological Survey: Reston, VA, USA, 1983; 50p.
45. Thompson, T.B.; Lyttle, T.; Pierson, J.R. *Genesis of the Bokan Mountain, Alaska, Uranium-Thorium Deposits*; United States Department of Energy: Washington, DC, USA, 1980; 232p.
46. De Saint-Andre, B.; Lancelot, J.R. Rb-Sr dating of the Bokan Mountain granite complex and its country rocks: Discussion. *Can. J. Earth Sci.* **1986**, *23*, 743–744. [CrossRef]
47. Pollock, J.C.; Sylvester, P.J.; Barr, S.M. Lu-Hf zircon and Sm-Nd whole-rock isotope constraints on the extent of juvenile arc crust in Avalonia: Examples from Newfoundland and Nova Scotia, Canada. *Can. J. Earth Sci.* **2015**, *52*, 161–181. [CrossRef]
48. De Paolo, D.J. *Neodymium Isotope Geochemistry: An Introduction*; Springer: New York, NY, USA, 1988; 187p.
49. De la Roche, H.; Leterrier, J.; Grandclaude, P.; Marchal, M. A classification of volcanic and plutonic rocks using R_1R_2-diagram and major-element analyses—Its relationships with current nomenclature. *Chem. Geol.* **1980**, *29*, 183–210.
50. Frost, B.R.; Barnes, C.G.; Collins, W.J.; Arculus, R.J.; Ellis, D.J.; Frost, C.D. A geochemical classification for granitic rocks. *J. Petrol.* **2001**, *42*, 2033–2048. [CrossRef]
51. Dall'Agnol, R.; de Oliveira, D.C. Oxidized, magnetite-series, rapakivi-type granite of Carajas, Brazil: Implications for classification and petrogenesis of A-type granites. *Lithos* **2007**, *93*, 215–233. [CrossRef]
52. Boynton, W.V. Cosmochemistry of the rare earth elements; meteorite studies. In *Rare Earth Element Geochemistry*; Henderson, P., Ed.; Elsevier: Amsterdam, The Netherlands, 1984; pp. 63–114.
53. McDonough, W.F.; Sun, S.-S. The composition of the Earth. *Chem. Geol.* **1995**, *120*, 229–253. [CrossRef]
54. Hilchie, L.; Russell, J.K.; Stanley, C.R. Unification of isocon and Pearce Element Ratio techniques in the quantification of material transfer. *Econ. Geol.* **2018**, *113*, 1603–1608. [CrossRef]
55. Gervasoni, F.; Klemme, S.; Rocha-Junior, E.R.V.; Berndt, J. Zircon saturation in silicate melts: A new and improved model for aluminous and alkali melts. *Contrib. Mineral. Petrol.* **2016**, *171*, 12. [CrossRef]
56. Watson, E.B.; Harrison, T.M. Zircon saturation revisited: Temperature and composition effects in a variety of crustal magma types. *Earth Planet. Sci. Lett.* **1983**, *64*, 295–304. [CrossRef]
57. Boehnke, P.; Watson, E.B.; Trail, D.; Harrison, T.M.; Schmitt, A.K. Zircon saturation re-revisited. *Chem. Geol.* **2013**, *351*, 324–334. [CrossRef]
58. Miller, C.F.; McDowell, S.M.; Mapes, R.W. Hot and cold granites? *Implications of zircon saturation temperatures and preservation of inheritance. Geology* **2003**, *31*, 529–532.
59. Eby, G.N. Chemical subdivision of the A-type granitoids: Petrogenetic and tectonic implications. *Geology* **1992**, *20*, 641–644. [CrossRef]
60. Whalen, J.B.; Currie, K.L.; Chappell, B.W. A-type granites: Geochemical characteristics, discrimination and petrogenesis. *Contrib. Mineral. Petrol.* **1987**, *95*, 407–419. [CrossRef]
61. Dostal, J.; van Hengstum, T.R.; Shellnutt, J.G.; Hanley, J.J. Petrogenetic evolution of Late Paleozoic rhyolites of the Harvey Group, southwestern New Brunswick (Canada) hosting uranium mineralization. *Contrib. Mineral. Petrol.* **2016**, *171*, 1–20. [CrossRef]
62. Dostal, J.; Capedri, S. Partition coefficients of uranium for some rock-forming minerals. *Chem. Geol.* **1975**, *15*, 285–294. [CrossRef]
63. Dostal, J.; Dupuy, C.; Carron, J.P.; Le Guen Kerneizon, M.; Maury, R.C. Partition coefficients of trace elements: Application to volcanic rocks of St. Vincent, West Indies. *Geochim. Cosmochim. Acta* **1984**, *47*, 525–533. [CrossRef]

64. Monecke, T.; Kempe, U.; Monecke, J.; Sala, M.; Wolf, D. Tetrad effect in rare earth element distribution patterns: A method of quantification with application to rock and mineral samples from granite-related rare metal deposits. *Geochim. Cosmochim. Acta* **2002**, *66*, 1185–1196. [CrossRef]
65. Agangi, A.; Kamenetsky, V.S.; McPhie, J. The role of fluorine in the concentration and transport of lithophile trace elements in felsic magmas: Insights from the Gawler Range volcanics, South Australia. *Chem. Geol.* **2010**, *273*, 314–325. [CrossRef]
66. Drinkwater, J.L.; Calzia, J.P. *Geochemical Reconnaissance of Alkali Plutons on Prince of Wales Island, Southeastern Alaska; Alaska Department of Natural Resources, Geological and Geophysical Surveys*; U.S. Geological Survey: Reston, VA, USA, 1994; pp. 173–184.
67. Barker, J.C. *Rare Earth Element- and Yttrium-Bearing Pegmatite Dikes near Dora Bay: Southern Prince of Wales Island*; Open-File Rep. 19-90; United States Bureau of Mines: Washington, DC, USA, 1990; 41p.
68. Eakins, G.R. Uranium investigations in southeastern Alaska. *Alsk. Div. Geol. Geophys. Surv. Rep.* **1975**, *44*, 59.
69. Barker, J.C.; Mardock, C.L. Lithophile metal, REE-Y-Nb deposits on southern Prince of Wales Island, Alaska. In *Process Mineralogy VIII*; Carson, D.J.T., Vassiliou, A.H., Eds.; The Minerals, Metals and Materials Society: Pittsburgh, PA, USA, 1988; pp. 139–157.
70. Bala, S.A.; Holm-Denoma, C.S.; Neymark, L.A.; Taylor, C.D.; Pietruszka, A.J.; Driscoll, R.L. U-Pb zircon ages and mineralogy of the Dora Bay intrusive complex and heavy REE-bearing pegmatite dikes. *Geol. Soc. Am. Abstr. Programs* **2014**, *46*, 782.
71. Dostal, J.; Karl, S.M.; Friedman, R.; Mortensen, J.K.; Layer, P.W.; Ford, A.B.; Corney, R. Late Devonian syenitic intrusion from southeastern Alaska: Petrogenesis, tectonic implications, and rare metal metallogeny. *Lithos* **2021**, *396–397*, 106205. [CrossRef]
72. McCafferty, A.E.; Stoeser, D.B.; Van Gosen, B.S. Geophysical interpretation of U, Th, and rare earth element mineralization of the Bokan Mountain peralkaline granite complex, Prince of Wales Island, southeast Alaska. *Interpretation* **2014**, *2*, SJ47–SJ63. [CrossRef]

Disclaimer/Publisher's Note: The statements, opinions and data contained in all publications are solely those of the individual author(s) and contributor(s) and not of MDPI and/or the editor(s). MDPI and/or the editor(s) disclaim responsibility for any injury to people or property resulting from any ideas, methods, instructions or products referred to in the content.